Science Advances
AAAS

Supplementary Materials for

IL-6–GP130 signaling protects human hepatocytes against lipid droplet accumulation in humanized liver models

Marisa Carbonaro *et al.*

Corresponding author: Zhe Li, zhe.li@regeneron.com

Sci. Adv. **9**, eadf4490 (2023)
DOI: 10.1126/sciadv.adf4490

This PDF file includes:

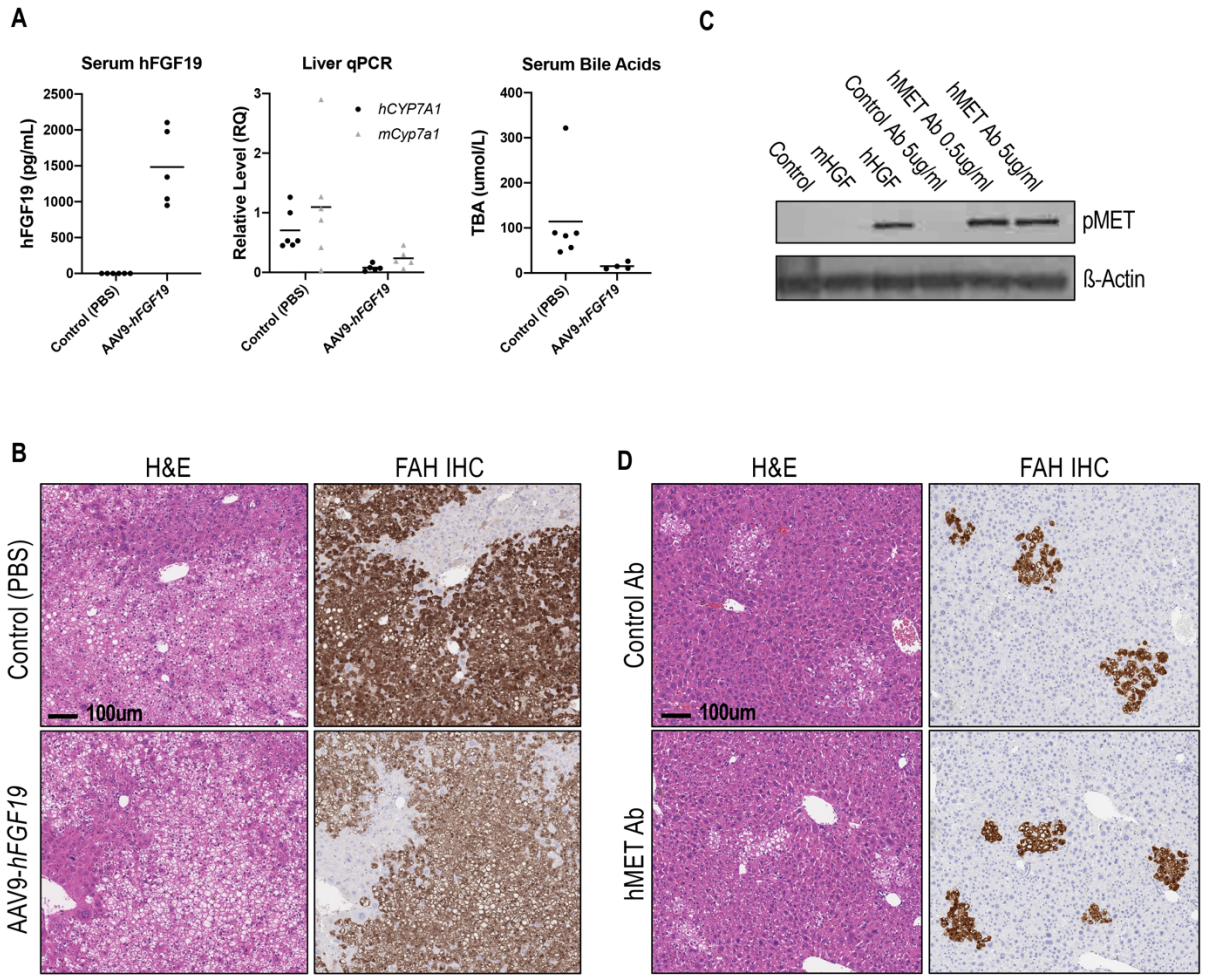

Figure S1. Restoration of FGF19-FGFR4 or HGF-MET signaling pathways do not correct lipid accumulation in human hepatocytes. A. AAV9-*hFGF19* treatment resulted in expression of hFGF19 protein, inhibition of the FGF19-FGFR4 target gene, *Cyp7a1*, expression in the liver and reduced bile acid production, as demonstrated by levels of hFGF19 in the serum (left panel), human *CYP7A1* and mouse *Cyp7a1* expression in the liver (middle panel; levels normalized to human and mouse *GAPDH*, respectively) and total bile acid (TBA) levels (right panel) in mice treated with AAV9-*hFGF19* vs. PBS control at the time of hepatocyte transplant. Lines in each graph represent the mean value. **B.** AAV9-*hFGF19* treatment did not correct hepatosteatosis in humanized liver mice, as shown by H&E and FAH IHC in livers from control vs. AAV9- *hFGF19* treated mice. **C.** Human cMET activating antibody mimics hHGF to activate MET, as shown by pMET levels in mouse hepatocytes with the endogenous murine *cMet* replaced by the human *cMET* gene, treated with mouse or human HGF (50ng/ml), control antibody, or a human- specific cMET activating antibody for 15 minutes. **D.** Human cMET activating antibody treatment (25mg/kg, 1x/week) did not correct hepatosteatosis in humanized liver mice, as shown by H&E and FAH IHC.

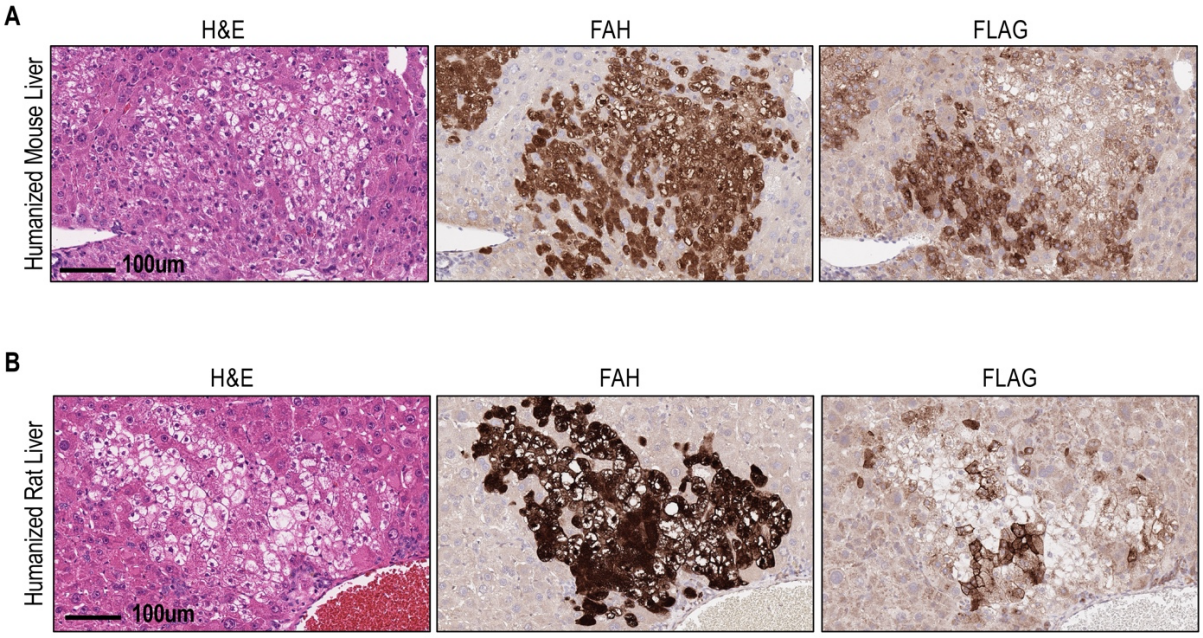

Figure S2. Expression of rodent IL6R in human hepatocytes eliminates lipid droplet accumulation in humanized livers. A & B. Ectopic expression of mouse (**A**) or rat (**B**) IL6R in human hepatocytes eliminates lipid droplet accumulation, as shown by H&E (left), FAH IHC (middle) and FLAG IHC (right) staining of nearby sections of *FSRG* mouse livers (**A**) or *FRG* rat livers (**B**) engrafted with PHH infected with lentivirus carrying *mIl6r* or *rIl6r*, respectively. mIL6R- or rIL6R-expressing human hepatocytes are positive for both FAH and FLAG IHC, while non-transduced human hepatocytes are FAH positive, but FLAG negative. Non-engrafted regions (endogenous mouse or rat cells) are negative for both FAH and FLAG IHC.

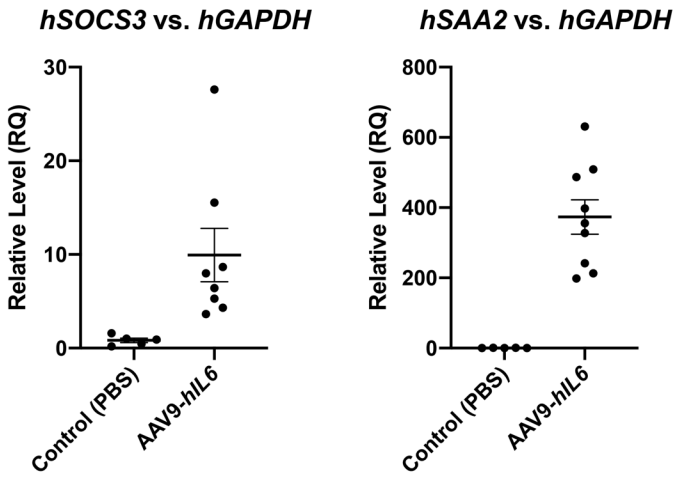

Figure S3. hIL6 over-expression by AAV can signal to engrafted human hepatocytes in humanized liver mouse model. AAV9-*hIL6* treatment led to activation of IL6 target genes in humanized livers, as shown by RNA levels of human *SOCS3* (left) and *SAA2* (right), in the livers of AAV9-*hIL6* treated mice, measured by TaqMan qPCR (plotted as mean ± SD).

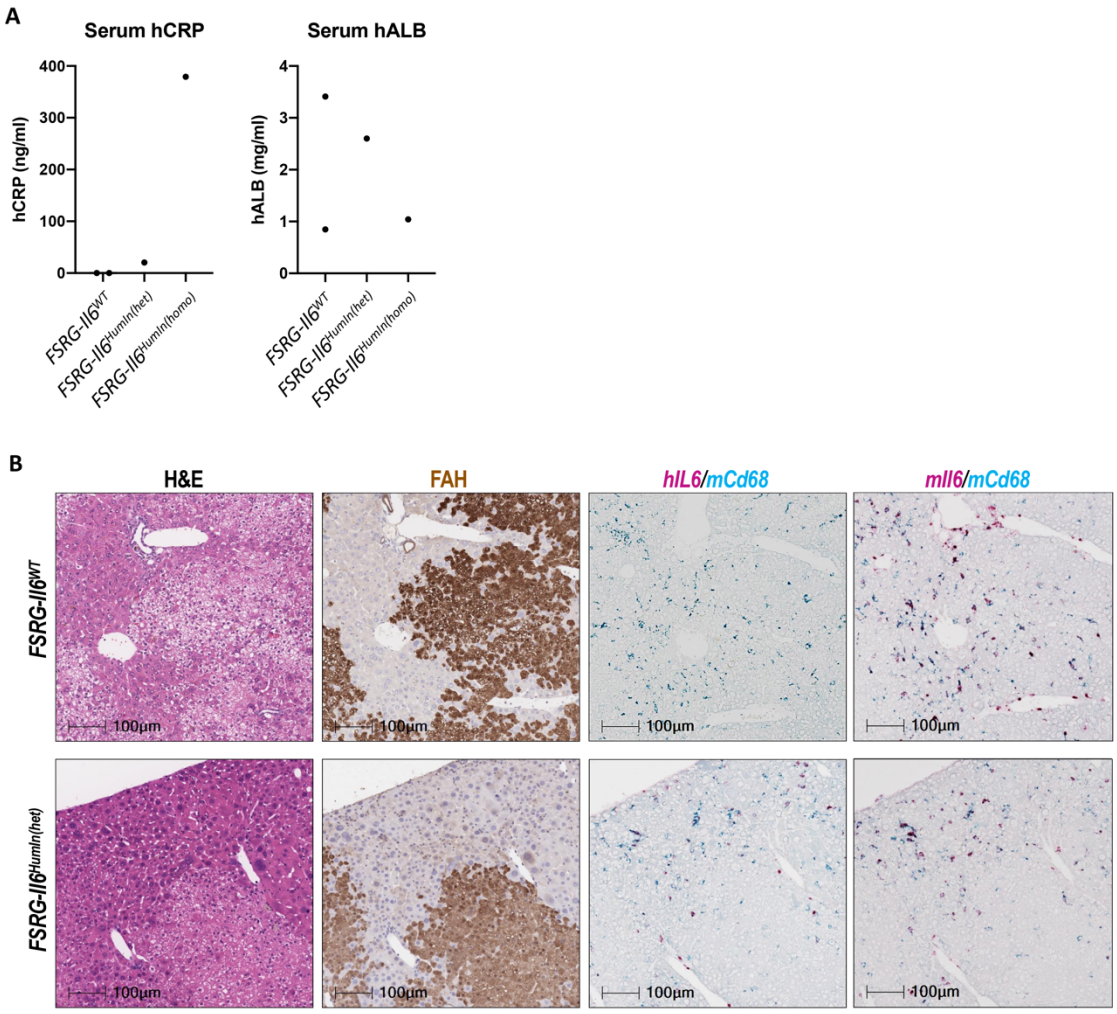

Figure S4. IL6 expression and signaling in the livers of *FSRG-hIL6* mice. A. Humanization of *Il6* allele led to a human specific hepatic IL6 response, shown by hCRP expression in *FSRG- Il6*$^{HumIn(het)}$ and *FSRG-Il6*$^{HumIn(homo)}$, but not *FSRG-Il6*^{WT} humanized liver mice (left). Engraftment of human hepatocytes was confirmed by serum hALB (right). **B.** Human *IL6* was detected (predominately in *Cd68* positive cells) in the livers of *FSRG-Il6*$^{HumIn(het)}$, but not *FSRG-Il6*^{WT} humanized liver mice after 2hr LPS stimulation, as shown by H&E, FAH IHC, *hIL6* (pink), *mIl6* (pink) and *mCd68* (blue) RNAscope staining.

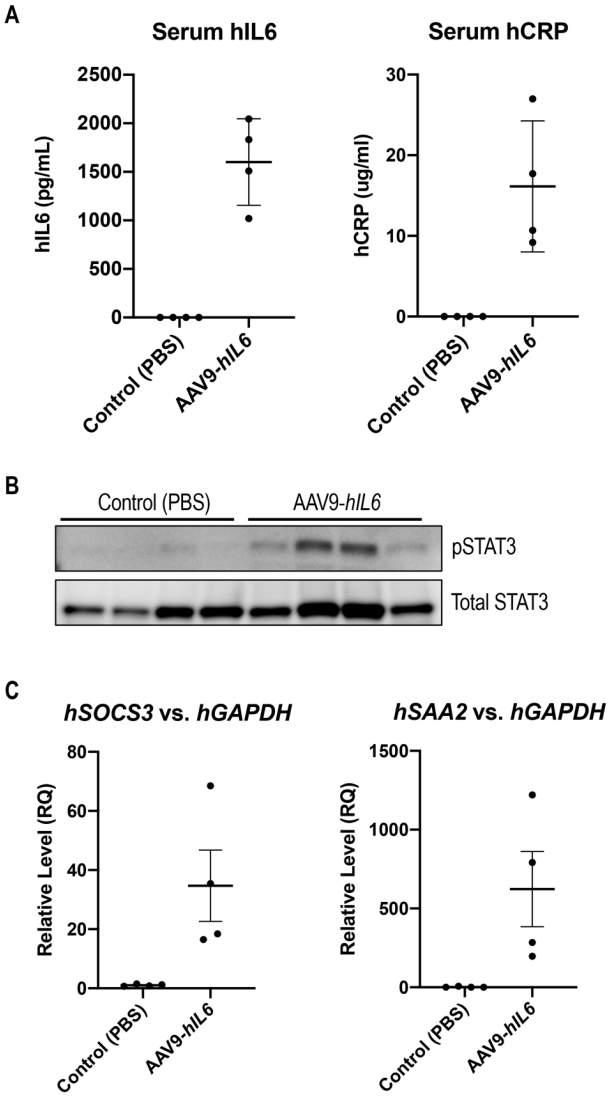

Figure S5. AAV9-*hIL6* dosing activates IL6 signaling in humanized liver mice. Humanized liver mice were treated with AAV9-*hIL6* or PBS control 8 weeks after PHH transplantation, and collected 4 weeks after AAV dosing. **A.** AAV9-*hIL6* dosing resulted in expression of hIL6 (left) and prototype acute phase reactant hCRP (right) in the serum of humanized liver mice. **B & C.** AAV9-*hIL6* dosing resulted in activation of hepatic IL6 pathway, as shown by a pSTAT3 Western blot of protein extracts (**B**), and RNA expression of IL6 target genes, *SOCS3* and *SAA2* (**C**) in humanized mouse livers treated with AAV9-*hIL6* vs. control PBS. Data plotted as mean ± SD.

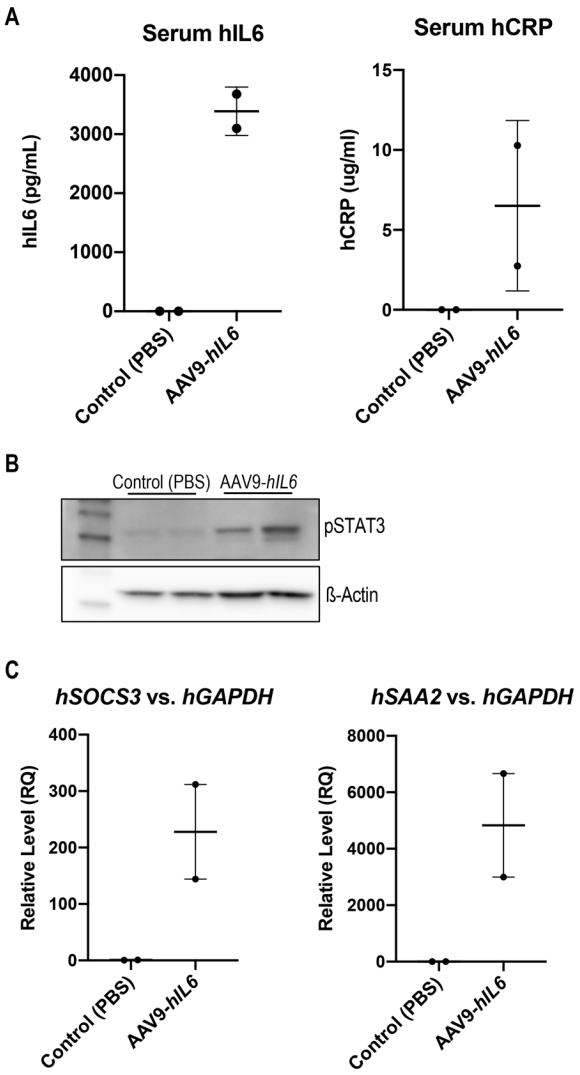

Figure S6. AAV9-*hIL6* treatment in humanized liver rats. Humanized liver rats were treated with AAV9-*hIL6* or PBS 12 weeks after PHH transplant, and collected 4 weeks after AAV dosing. **A.** AAV9-*hIL6* dosing resulted in expression of hIL6 (left) and prototype acute phase reactant hCRP (right) in the serum of humanized liver rats. **B & C.** AAV9-*hIL6* dosing resulted in activation of hepatic IL6 pathway, as shown by a pSTAT3 Western blot of protein extracts (**B**) and RNA expression of IL6 target genes, *SOCS3* and *SAA2* (**C**), in humanized rat livers treated with AAV9-*hIL6* vs. control PBS. Data plotted as mean ± SD.

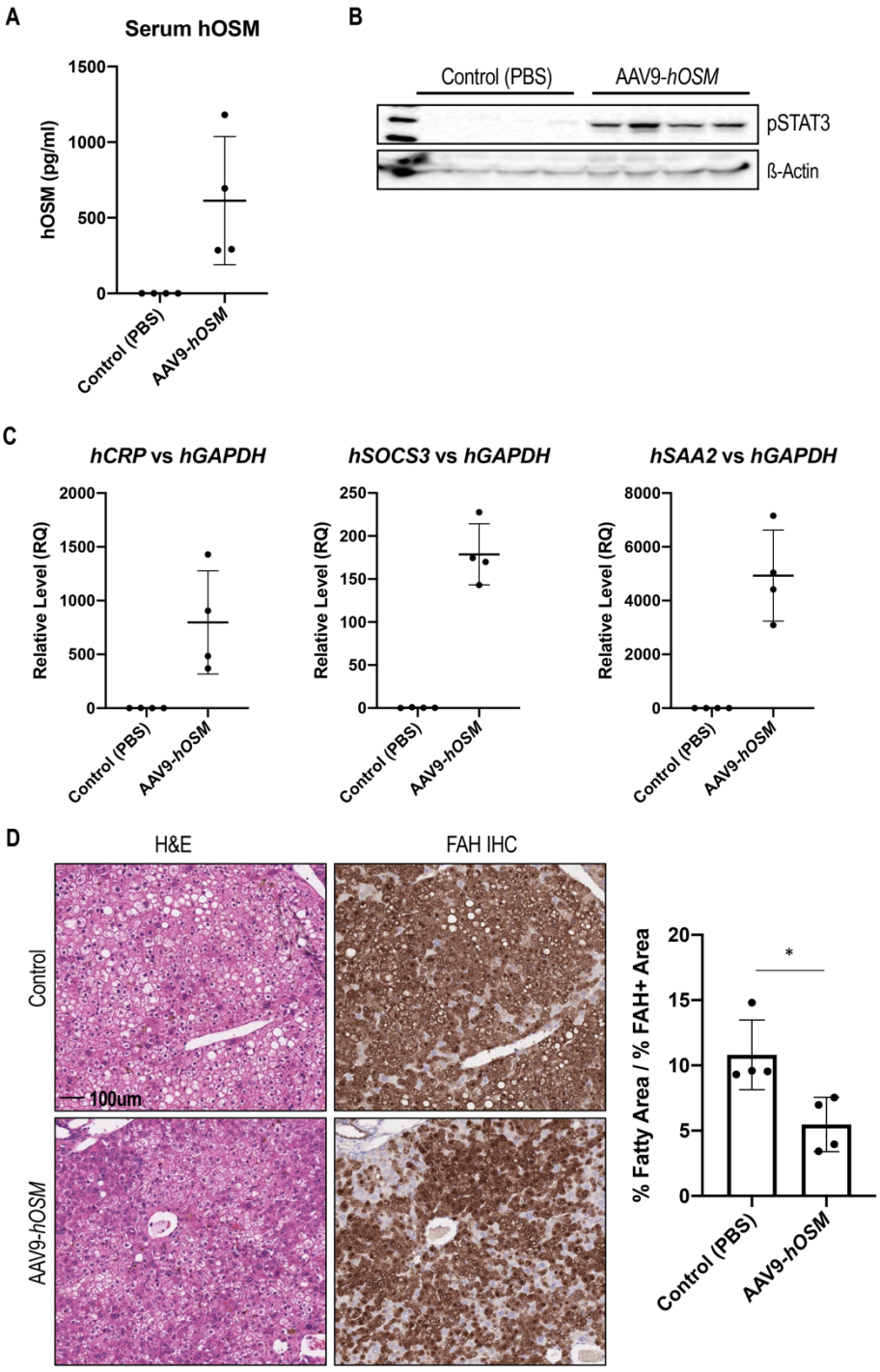

Figure S7. Human OSM over-expression also corrects lipid droplet accumulation in engrafted human hepatocytes. Humanized liver mice were treated with AAV9-*hOSM* or PBS control 12 weeks after PHH transplantation, and collected 3 weeks after AAV dosing. **A.** hOSM levels in the serum of humanized liver mice at the time of termination. **B.** Western blot of liver lysates confirming activation of pSTAT3 in AAV9-*hOSM* treated mice. **C.** RNA expression of human target genes, *CRP*, *SOCS3* and *SAA2* in AAV9-*hOSM* treated versus control mice, confirming activation of downstream gp130 signaling. **D.** H&E staining and FAH IHC on liver sections from AAV9-*hOSM* and PBS treated mice. Quantification of the % fatty area (negative H&E staining) over % positive FAH staining shows mean ± SD (each dot represents one mouse, 2 liver lobes/mouse were analyzed). * $p<0.05$, Unpaired *t* test.

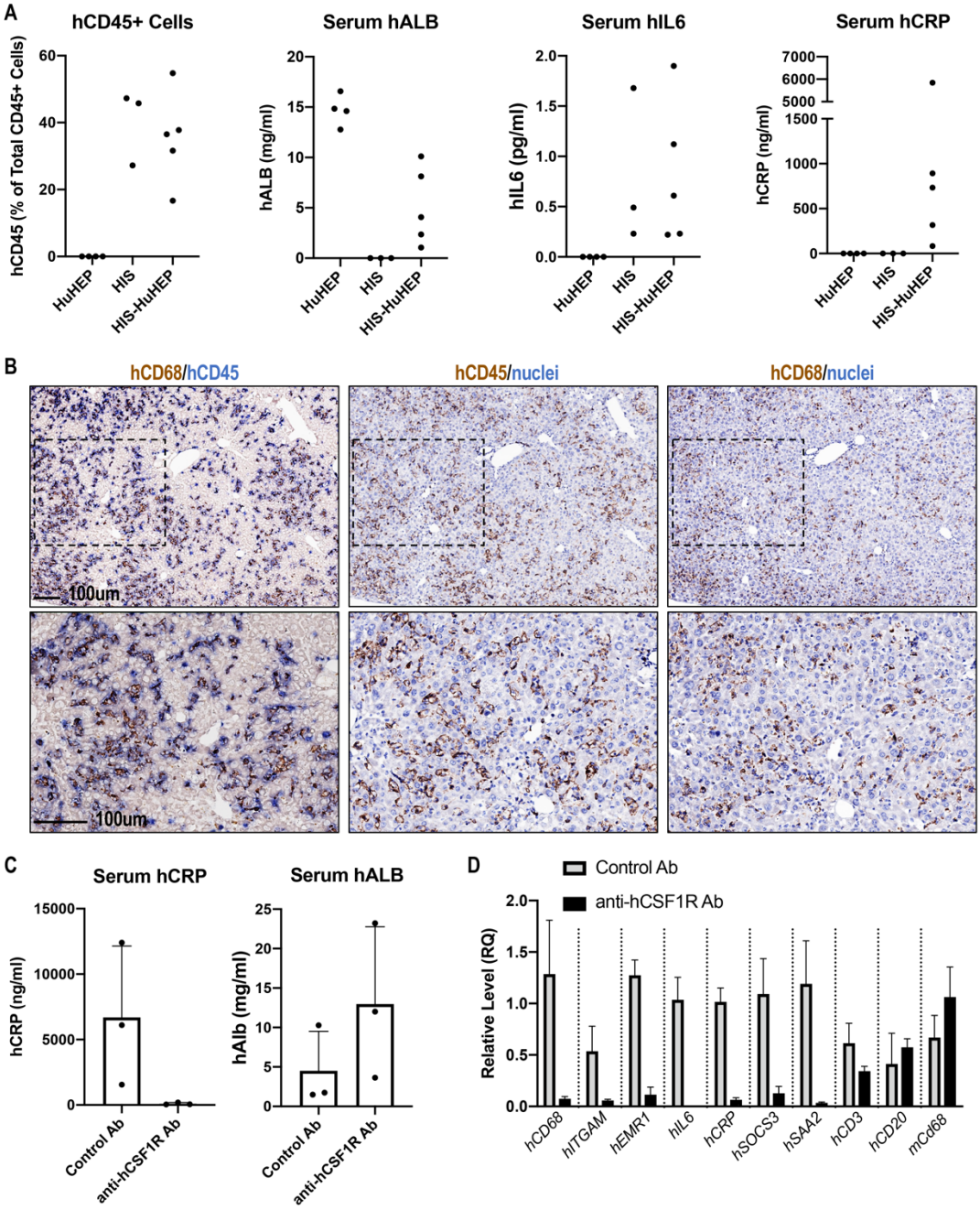

Figure S8. Engraftment of human immune cells led to hIL6 expression in HIS-HuHEP mice. A. Human immune cell engraftment shown by hCD45+ cells in the peripheral blood of HIS and HIS-HuHEP, but not HuHEP mice (left panel). Human hepatocyte engraftment was shown by serum human albumin in HuHEP and HIS-HuHEP, but not HIS mice (second panel). hIL6 expression was detected in the serum of HIS and HIS-HuHEP, but not HuHEP mice (third panel). Hepatic IL6 target gene, hCRP, was detected only in the serum of HIS-HuHEP mice, with both human immune cells and human hepatocytes (right panel). **B.** Single and double-IHC for hCD45 and hCD68 in nearby sections from HIS-HuHEP mouse livers. Double staining (left panels) confirms that the majority of hCD45+ cells (blue) are also hCD68+ (brown). **C.** Anti-hCSF1R treatment led to complete absence of hCRP in HIS- HuHEP mice, as shown by hCRP ELISA (left), despite high liver humanization as indicated by human albumin levels (right). **D.** Anti-hCSF1R treatment led to depletion of human macrophages, but not other immune cells, as shown by RNA expression of human macrophage markers (*hCD68, hITGAM, hEMR1*), *hIL6*, *hCD3*, *hCD20* and mouse *Cd68* in livers of control or anti-hCSF1R antibody treated HIS-HuHEP mice. Data in **C** & **D** shown as mean ± SD.

Gene	Probe Sequence	Forward Primer	Reverse Primer
hIL6	CGGCATCTCAGCCCTGAGAAAGGA	TGACAAACAAATTCGGTACATCCTC	GTGCCTCTTTGCTGCTTTCAC
hSOCS3	TCCAAGAGCGAGTACCAGCTGG	TGCGCCTCAAGACCTTCAG	TCACTGCGCTCCAGTAGAAG
hSAA2	AATATCCAGAGACTCACAGGCCGTGG	GGCTGCAGAAGTGATCAGCAATG	ATCGGCCAGCGAGTCCTC
hCRP	TGTCTGGTCTGGGAGCTCGTTAAC	AGCGCCTGAGAATGGAGGTAA	TGGACCGTTTCCCAGCATA
hCD68	AACAGCACTGCCACCAGCCCAG	GCCACGGTTCATCCAACAAG	GGTGGGCAGAACTGGTGAATC
hITGAM	CCTCTCACTCCGACTTTCTGGCTGA	TGCCACACCAAGGAGCG	GTTGCCTTTGAGGGTAGCATTG
hEMR1	CCACACGGAAACCAAACACAAAGGG	AGCTGGGAAGGGCACATAAGAC	GCTGGGCACAAGGTACTG
hCD3	TCCAGAGACAACGCCAAGGATTCC	GAAGGGCCGATTCACCATC	TGCAGCTCTCAGACTGTCCAT
hCD20	TGCTATGCAATCTGGTCCAAAACCAC	CCGGCAGAGCCAATGAAAGG	GGCCCACCAGTGAAGACATC
mCd68	CTTCCCACAGGCAGCACAGTGG	GGCGGTGGAATACAATGTGTC	GGAGCTCTCGAAGAGATGAATTCTG
hCYP7A1	CCCTCAACATCCGGACAGCTAAGGA	GAATCGCTGAGGCTTTCCAGTG	ACCGTCCTCAAGGTGCAAAGTG
mCyp7a1	CAAGAACCTGTACATGAGGGACCAGG	GGCTGGCTGAGAGCTTGA	GGTGGAGAGTGTATCGTTGAGAA
hGAPDH	TCAACAGCGACACCCACTCCTC	CCAGGTGGTCTCCTCTGACT	GCTTGACAAAGTGGTCGTTGA
mGapdh	ATCCACTGGTGCTGCCAAGGCTG	TGCCCAGAACATCATCCCT	GGAAGGCCATGCCAGTGAG

Table S1: Primer and probe sequences used for RT-PCR.